Nanocrystalline Anatase Titania Thin Films Synthesized by Spray Pyrolysis for Gas Detection

M.Z. Obida[1], H.H. Afify[1], M.O. Abou-Helal[1], and H.A.H. Zaid[2]

[1] *Physics Dept., Solid State Division, National Research Center NRC, 12622 Dokki, Cairo, Egypt.*
[2] *Physics Dept., Science, Arts and Education Faculty of Girls, Ain-Shams Uni., Heliopolis, Cairo, Egypt.*

Nanocrystalline (NC) materials are exhibiting small particle size and large surface area which may be applied for gas sensors. Nano-crystalline TiO_2 films are synthesized by spray pyrolysis technique. The XRD investigation for the deposited films shows that they have only polycrystalline anatase phase with nano-size. The AFM photographs reveal the nano-size of the constituents. The crystallite size and crystallinity of the samples are discussed with respect to the film thickness and deposition temperature. The dc resistivity dependence on temperature for samples is studied and correlated with the preparation parameters. The sample resistance is measured in the presence of technologically important gases CO, O_2 and H_2. The sensitivity and response time of the samples to the tested gases are assigned at varied operating temperature. It is found that optimum operating temperature for H_2 and CO is 330^oC and 310^oC, respectively. Also, the maximum sensitivity is 90% and 70%, and the response time is about 8 and 3 seconds for H_2 and CO respectively, at the proceeding operating temperature.

1. Introduction:

Nano-crystalline materials with particle size smaller than 100 nm exhibit amazing properties which are not found in conventional materials [1]. One of the distinctive features, the main one for gas sensors, is an extremely large specific surface area. Oxide semiconductor films are promising for gas sensors due to the dependence of their electrical conductivity on the environmental gases such as O_2, CO, H_2……[2].

Titanium dioxide is being used in a great variety of applications. It has been investigated for humidity and gas-sensing behavior [3,4]. It has three

different crystallographic forms: brookite, anatase and rutile. Anatase is metastable and converted irreversibly into rutile at high temperature. Its preparation is fundamental to obtain properties suitable for gas-sensing applications such as: structural stability, porosity and high surface-to-volume ratio in order to emphasize surface effects. The sensing properties of TiO_2 films are based on surface interactions of reducing or oxidizing species, which affect the conductivity of the films.

Films of nano-sized TiO_2 could be achieved by different techniques such as sputtering in reactive atmosphere followed by thermal annealing at 800°C, Sol-Gel, Spray Pyrolysis, Screen Printing, Laser Ablation, …. etc. The main purpose of this paper is to prepare low cost nano-sized TiO_2 films with structural and electrical characteristics suitable for sensing oxidizing and reducing gases.

2. Experimental:

A developed spray pyrolysis setup has been designed and assembled to overcome limitations of previous systems such as repeatability and homogeneity of the deposited films. The system is almost fully computerized and consists of the following components: PC-controlled x-y table, digital temperature controller, digital gas flow meter and digital solution pump. Most of these components are working alone with built in processors, and/or are controlled by PC. A schematic diagram of the used system is given in Fig (1).

The TiO_2 films were deposited on 2.5x1.5x0.1 cm^3 glass substrates, after applying the conventional cleaning procedures. This type of glass (Menzel-Gläser, Germany) is stable till more than 600°C. It has a lower cut off wavelength ($\approx$280 nm), which far away from that of the prepared TiO_2 ($\approx$325 nm), and also it is not expensive which makes the produced films more attractive for industrial applications. The deposition parameters are: 0.8 M solution composed of chemically pure $TiCl_4$ dissolved in ethanol. Filtered air is used as a carrier. The solution and gas flow rates are 0.7 ml/hr and 25 l/hr, respectively, the substrate temperature range is 325-475°C and the spray time range is 5-30 minutes.
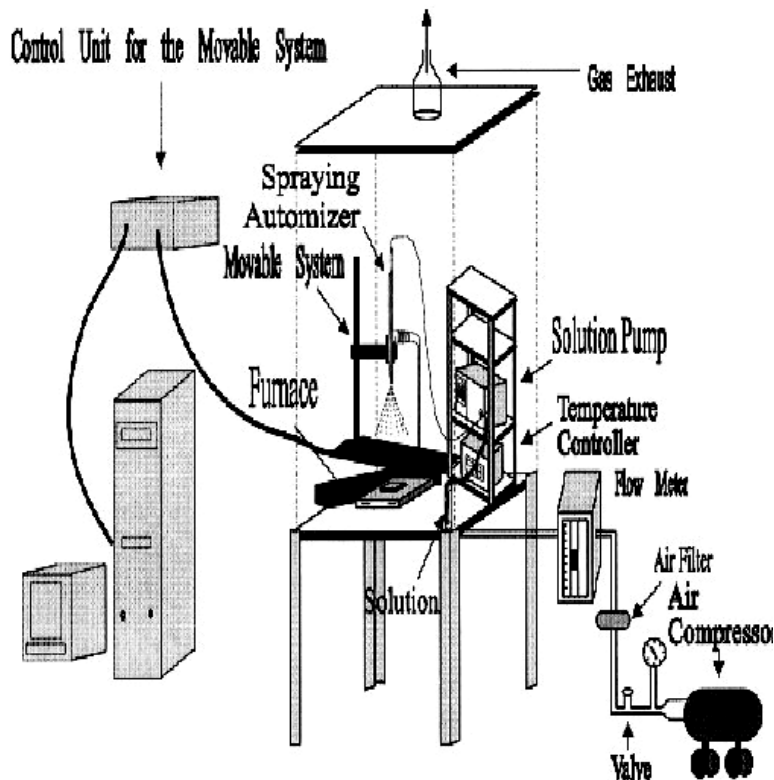
Fig. (1): The movable and computerized spray pyrolysis system with X-Y table.

X-ray diffraction was used to elucidate the structure of the prepared films. The as-deposited films were subjected to structural analysis using (Diano corroboration-USA equipment with CO k_α radiation). The diffraction patterns were recorded automatically with a scanning speed 8deg/min and scanning angular range ($2\theta=4^{\circ}$to 90°), $\lambda=1.514184$ (Å). The atomic force microscope (AFM) studies are carried out in the National Institute of Standards (Egypt). The deposited samples are imaged in contact mode. The images presented here are submitted to a flatness process. The crystallite diameter is measured on the original image before the flatness process. The film thickness is measured in the National Institute of Standards by Interference Microscope for samples have an edge and coated with Ag film. The gas sensing properties of the deposited films toward oxygen, hydrogen and carbon monoxide (CO) are measured at controlled humidity (RH 35%) and the temperature of the chamber containing the sensor was maintained at the operating temperature. The changes in the sensor electrical resistance due to variations of the surrounding atmosphere have been recorded and monitored by METEX (PC interface Multimeter Peak Tech 4370). Dry carbon monoxide gas generation system was made to obtain CO gas

from chemical reaction of sodium formate (NaCOOH, Fine chem. LTD) and sulphuric acid (H_2SO_4, 98%). The produced CO volume is determined from the following equation:

$$2NaCOOH + H_2SO_4 \rightarrow Na_2SO_4 + 2CO\uparrow + 2H_2O$$
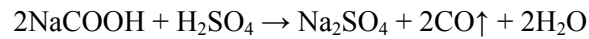
The other two gases (O_2 & H_2) are fed from their corresponding cylinders.

3. Results and Discussion:

3.1. Film Structure

The X-Ray diffraction (XRD) analysis is conducted to determine the phases and the grain size. The XRD patterns for the investigated samples prepared at different deposition temperatures and constant deposition time as well as those deposited at different deposition times and constant deposition temperature are shown in Fig.(2 a,b).
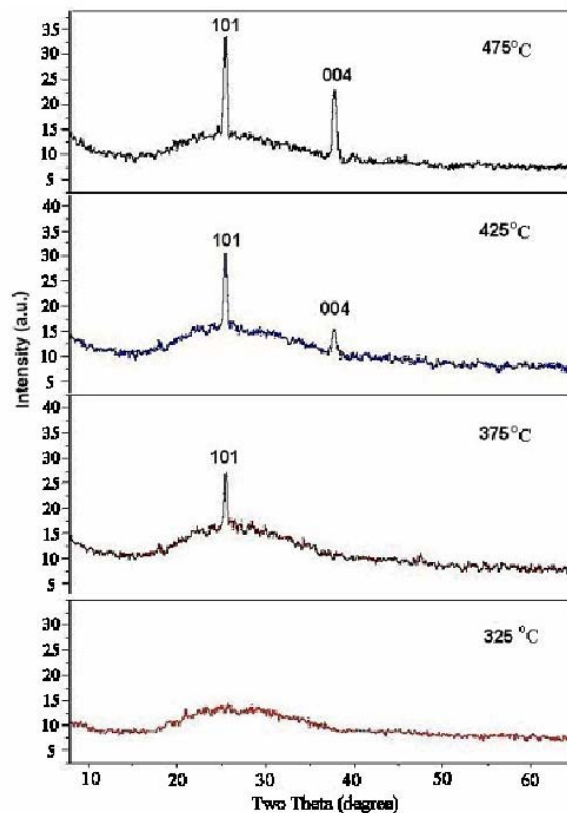

Fig. (2a): XRD of TiO_2 films deposited at different deposition temperature and 30 min spray time.
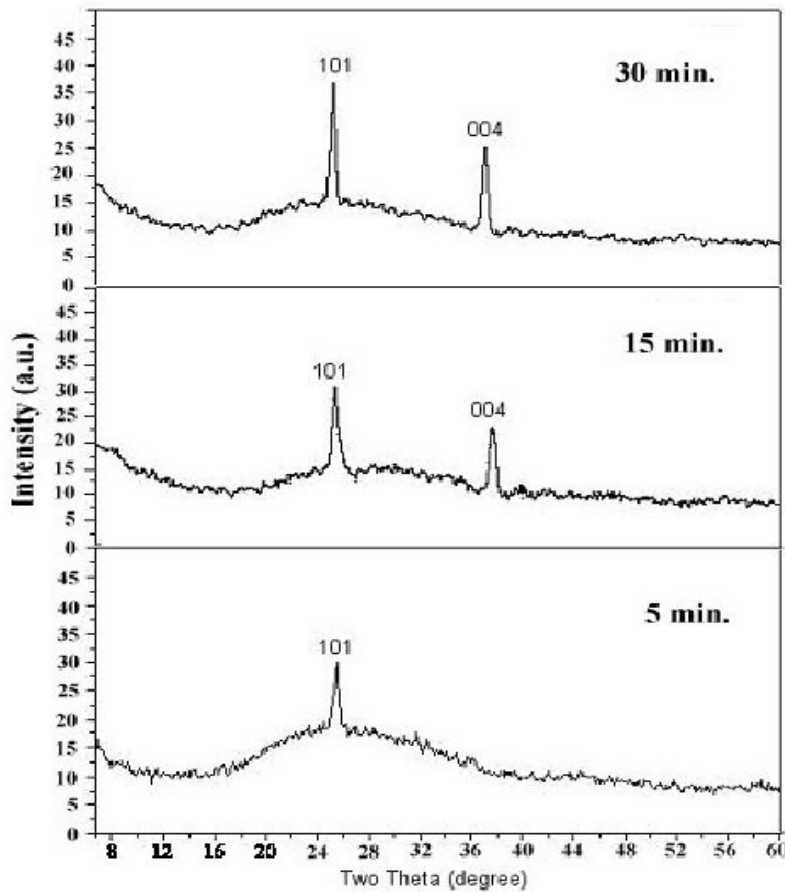
Fig. (2b): XRD patterns of TiO$_2$ thin films deposited at constant substrate temperature (500°C) and different deposition time.

It is clear that the samples deposited at 325°C shows a broad hump at 2θ (20-30), which indicating the amorphous structure. In order to have a clear cut decision GIXRD and/or ED has to be used, unfortunately, we do not have either facilities. The XRD patterns for samples prepared at temperatures > 325°C show only two peaks, their intensities increase as the deposition temperature and time increase. These peaks are indexed with the standard JCPDS (21-1272) and found to be corresponding to (101) and (004) anatase phase [5-7]. The phase diagram of Ti-O compound [10] reported that the rutile is formed at above 800°C in most probable to equilibrium conditions. Therefore, only the anatase phase is obtained since the covered range 325-475°C of substrate temperature, is still insufficient to grow rutile phase. The mean crystallite size has been obtained with Scherer relation [11],

$$D = k\lambda / (\beta Cos\theta)$$

where D is the crystallite size, k is a fixed number of 0.9, λ is the X-ray wavelength, θ is the Bragg's angle in degrees, and β is the full-width-at-half-maximum (FWHM) of the chosen peak, and equal to B_{sample}-$B_{instrument}$, where B is the broadening. The instrumental broadening was done using the free strain quartz sample delivered by Diano Corporation by using the same condition conducted for the experiment. Using FWHM values of the (101) reflection, the values for representative investigated samples, are given in Table (1). The crystallite size increases from 17 to 21 nm at 375°C up to 475°C, respectively.

Table (1): Values of crystallite size

Temperature (^{o}C)	Crystallite size (nm)
375	17
425	19
475	21

Atomic Force Microscopy (AFM) images from samples prepared at 375, 425 and 475°C and deposition time 30 minutes are reported in Fig.(3). It shows that the films are composed of small crystallites. The average crystallite diameters are 20, 23 and 28 nm, respectively. These values are larger than the size measured with XRD. As XRD is sensitive to the crystallite thickness perpendicular to the film and the AFM image show the film surface, therefore, the grains are larger at the film surface than that at the inner regions.

3.2. DC Electrical Properties

The undoped TiO_2 consists of non-stoichiometric TiO_2, which contains bulk oxygen vacancies and interstitial oxygen ions, that act as donor states. These states permit the adsorption of oxygen. When oxygen molecule gets adsorbed at the TiO_2 film surface or at the grain boundaries, it extracts electrons from the conduction band, thus, reducing the concentration of the electrons which allowing an increase in the film resistivity [8]. As adsorbed oxygen concentration increases, the number of conduction band electrons decreases further and the TiO_2 film become more resistive [12].

It is found that [13] when TiO_2 film, prepared by sputtering technique on fused quartz substrates, exposed to heating-cooling thermal cycles in air and vacuum between 25 and 400°C, the film resistivity at room temperature is increased after the cycling in air and is decreased after cycling in vacuum. This result had been explained by the oxidation during heating-cooling cycle in air and the reduction in vacuum. Thus, oxidation of the film decreases the number of free carriers whereas reduction increase it.
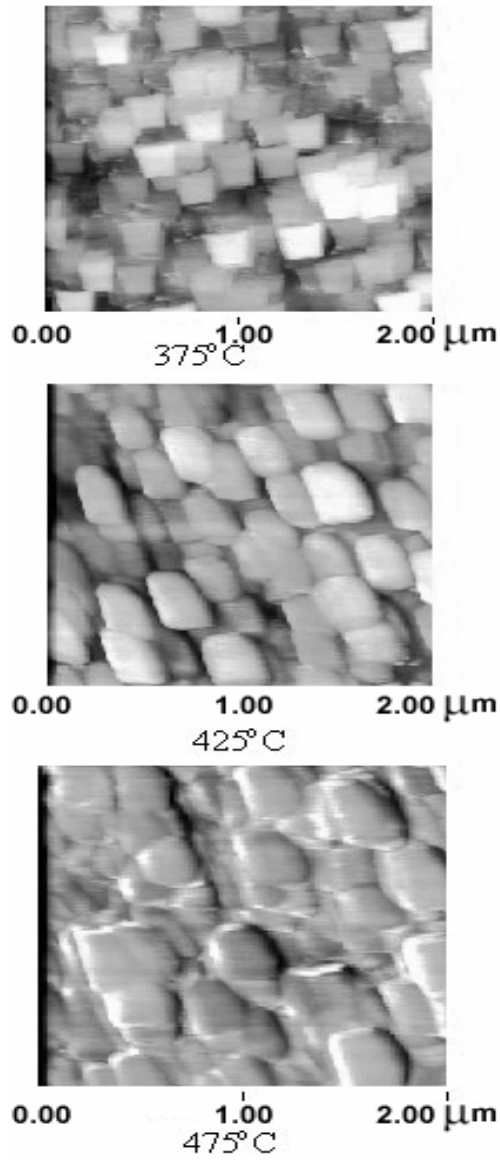
Fig. (3): AFM images for Tio$_2$ film prepared at (375, 425 and 475°C) and 30 min.

In this work the dc electrical resistivity versus temperature from 25 up to 400°C is studied for TiO$_2$ films deposited at (10 and 30 minutes) and different deposition temperatures at each deposition time. At each test temperature, we wait 10 minutes to attain a constant value of the resistance before recording. A representative curve for the change of the film resistance with the time at constant test temperature is shown in Fig.(4).
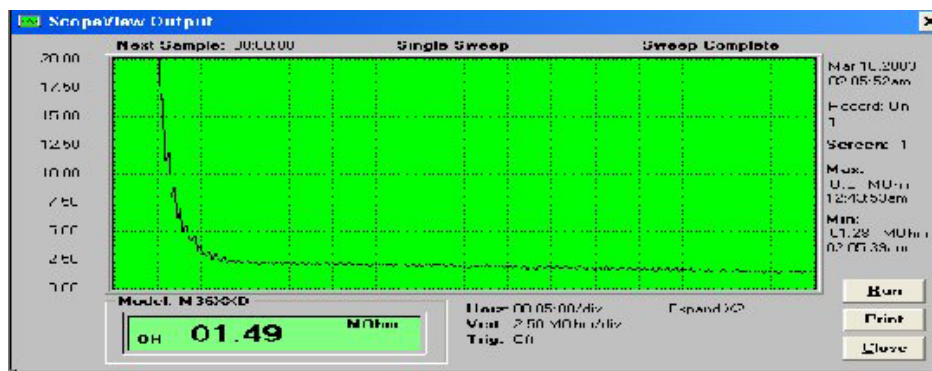
20 min.

Fig. (4): Effect of time of film resistance at operating temperature 3000°C for TiO$_2$ samples deposited at 375°C and 20 min.

The recorded data are modified by introducing sample dimensions to calculate the film resistivity and drawn it as a function of test temperature. It is clear from Fig.(5) that all the investigated samples show higher resistance at room temperature ($\approx 10^{12}\Omega$) which could not be detected by the recording device (METEX).
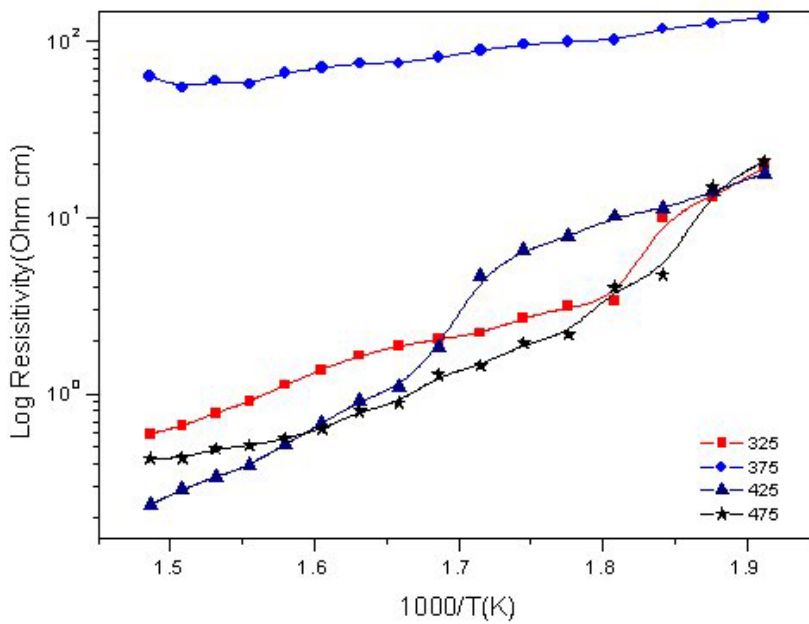

Fig. (5): Resistivity versus 1000/T (k) for TiO$_2$ films prepared at different deposition temperatures and constant spray time (10 min).

As the test temperature raised, the film resistance decreased. The TiO_2 films deposited at 375, 425 and 475°C at constant deposition time (30 & 10 min.), show almost the same trend of decreasing the resistivity with increasing the test temperature. The samples prepared at 325°C show high resistivity all over the covered temperature range compared with the samples prepared at temperatures higher than 325°C. This may be due to the structure of the TiO_2 films as revealed by their XRD, Fig.(2a).

It is worthy to pay attention that the TiO_2 films prepared at 325°C show about six order of magnitude lower resistance with raising the temperature from room temperature up to 400°C, while those samples prepared at deposition temperature higher than 325 show eight order of magnitude (10^{12} to $10^4\Omega$).

The higher resistivity for the investigated TiO_2 films regardless the preparation conditions could be explained as: during film deposition, it is quite likely that large numbers of oxygen molecules are adsorbed in the film both at grains boundaries and on the surface. The adsorbed oxygen will produce potential barriers which hinder the electron transport. Also, the adsorbed oxygen withdraws the electron from the conduction band allowing high resistivity.

The reversible decrease in TiO_2 film resistivity with increasing test temperature could be attributed to the evolution of the adsorbed oxygen at film surface and grain boundaries which allow the increase of electrons and decrease of the potential barrier at grain boundaries.

The determined activation energy from the slope in Fig.(5) is found to be (0.2 eV), which is smaller than the activation energy for intrinsic conduction. This make one conceive that adsorbed oxygen evolution by increases the film temperature is the main mechanism for the decrease of film resistivity. The evolution of oxygen from TiO_2 film when heated at elevated temperatures is reported in literature [14].

3.3. Effect of gases on dc electrical properties:

In this part, TiO_2 films deposited at 475°C and 30 minutes, since they have well defined crystallite shapes as revealed by AFM, is selected as model to study the effect of reducing (CO & H_2) and oxidizing (O_2) gases on its dc resistance. This study is devoted to explore to what extent the prepared samples could be used as sensors to these gases.

A home-made measuring system provided with oxygen, hydrogen cylinders with their manometer and CO glass reactor is used. All these gas

sources are connected to the system through a polyethelene pipe line $\approx$ 1.5 meter and with glass tapes. The results of the change in the film resistance with time of the TiO_2 films during their exposure to CO, H_2 and O_2 at different operating temperature are shown in Figs.(6,7,8).
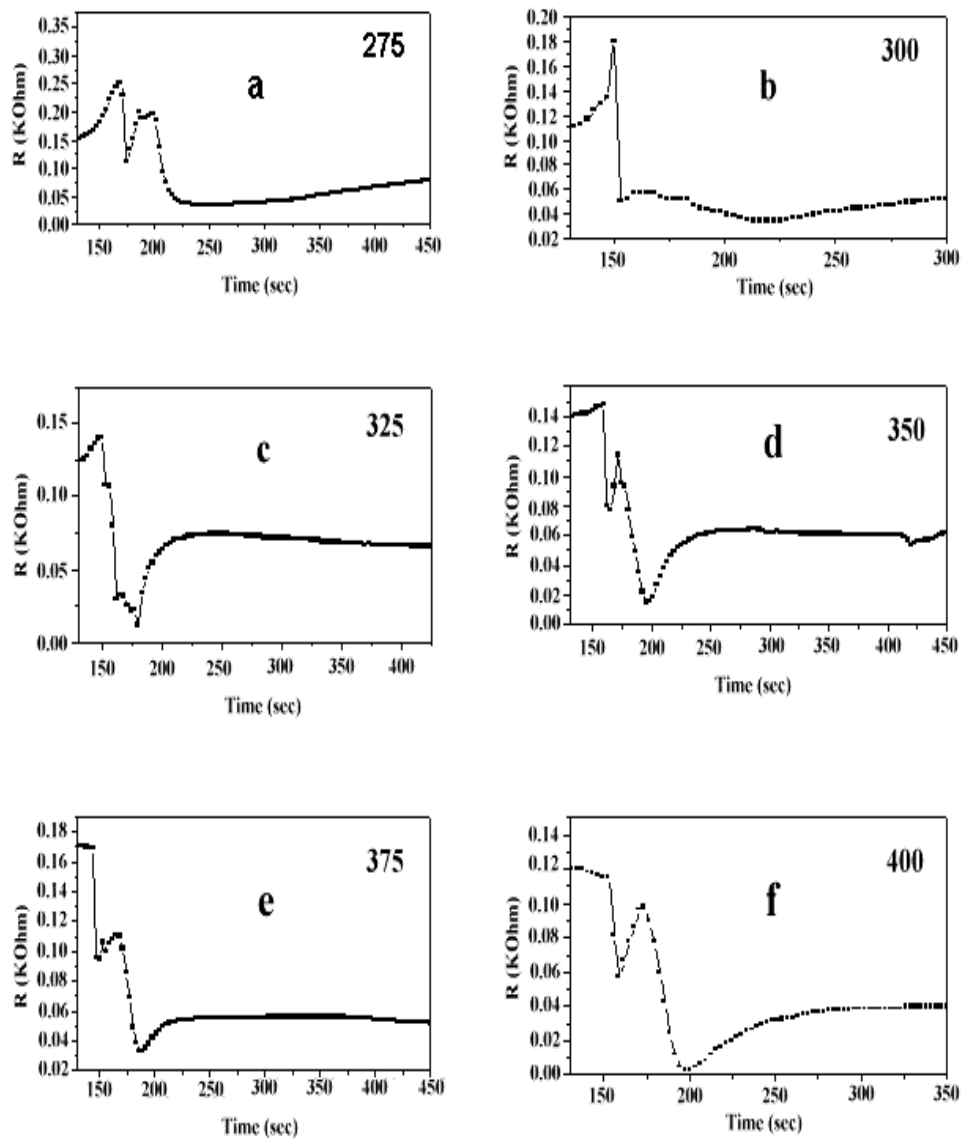

Fig. (6): Effect of CO gas on the resistance of TiO_2 prepared at 375°C and 30 main at different operating temperatures.
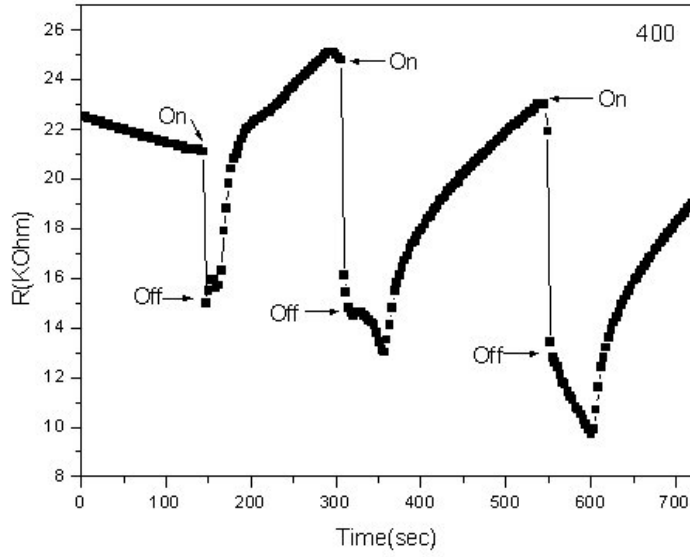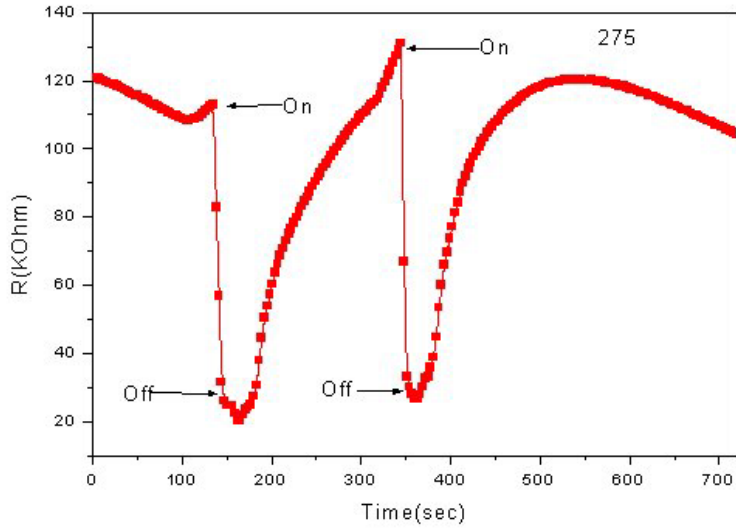
Fig. (7): The dynamic response for H_2 at two operating temperatures for TiO_2 prepared at 375°C and min.
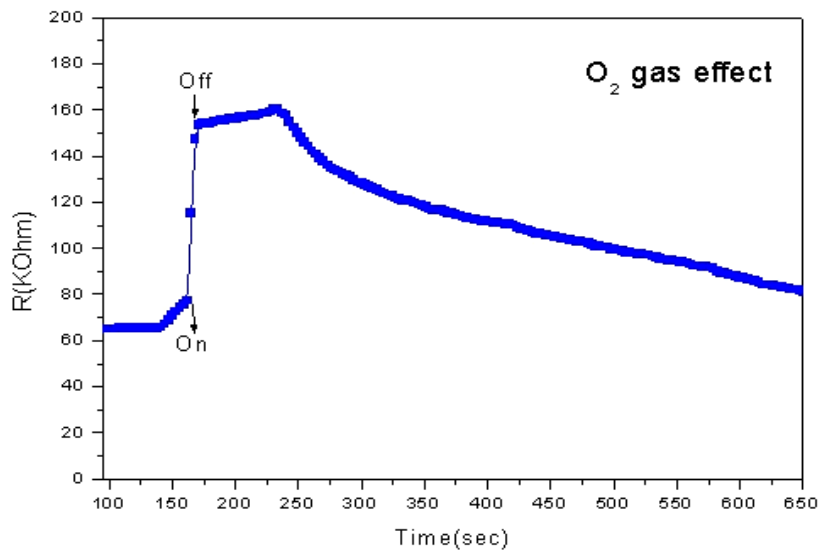
Fig. (8): The dynamic response for TiO_2 prepared at 375°C and 30 min., the operating temperature is 300°C.

3.3.1. Carbon monoxide:

a) dynamic response

The salient feature for the curve family of CO is the slight increase of the film resistance at the onset of the curve which decreases as the operating temperature increases. When the gas inlet is opened to the test chamber, it causes slight decrease of the operating temperature allowing the slight increase in the equilibrium resistance at the operating temperature. Since the flow of CO is constant at all operating temperatures, then the induced reduction in the operating temperature due to the gas rushing will decrease as the operating temperature decreases, as shown in Fig.(6).

Also, at higher operating temperatures a sudden decrease in film resistance is followed by a slight increase in film resistance followed by a sudden and continuous decrease in resistance. This is not observed at lower operating temperatures. This observation could be explained, as the operating temperature increases, the thermal flux opposes the gas stream at its entrance inducing little disturbance in the operating temperature causing the increase in film resistance.

Also, the observed slower recovery of the film resistance during the swept time (10 minutes) may be due to the loss of the sharp on-off cycle of the gas. This means that the generation of CO is strong and fades with time. The tiny residual of CO gas impede the recovery of the film resistance.

The sharp instantaneous decrease in the film resistance when exposed to CO gas could be rendered to the reaction of the CO gas with the adsorbed oxygen on the film surface and at the grain boundaries releasing the trapped electrons back to the film and increasing its conductivity. The obtained results are consistent with that expected based on concepts [15] and reported data in the literatures [16].

b) Sensitivity and response time

The sensitivity S is defined by the form:

$$S = (R_o - R_{gs})/R_{gs}$$

where R_o is the resistance of the sensor before passing the gas and R_{gs} that after passing it. Also, the response time, is defined as the time needed for the sample to reach 90% of the final signal for a given concentration of the gas.

The crystallite size and the gas concentration are constant while the operating temperature is varied. The sensitivity of the sample is calculated and traced as a function of operating temperature as shown in Fig.(9). The error bars on the graph indicate that the degree of repeatability upon measurements of three fresh TiO_2 films prepared at 475^oC and 30 minutes. The samples show high sensitivity to CO gas at the vicinity of 310^oC. The response time for CO at low operating temperature is 3 seconds as shown in Fig.(10).

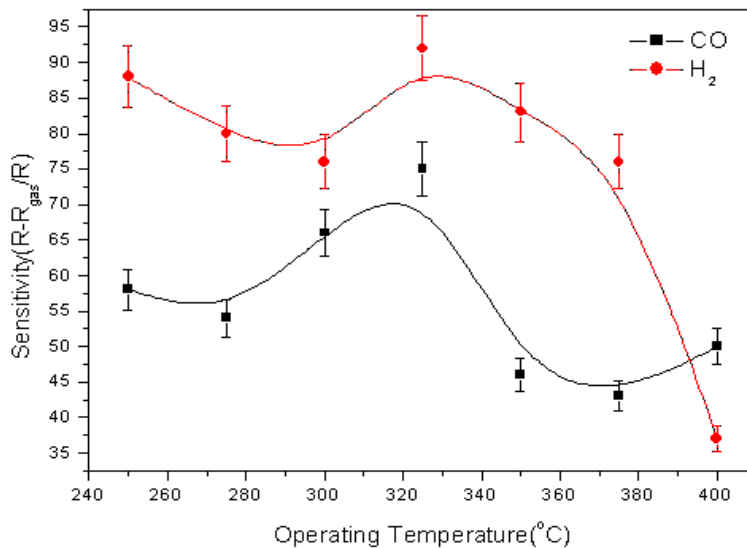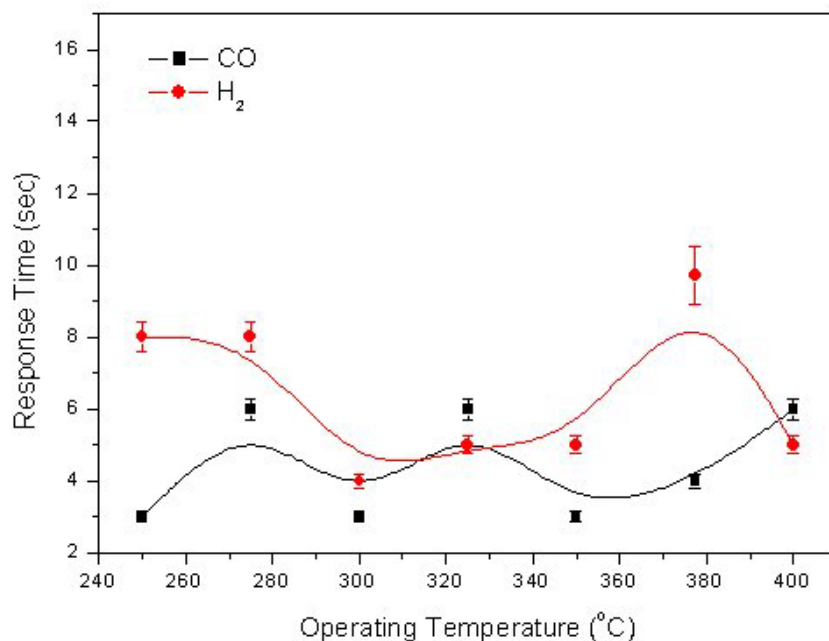**Fig. (9):** TiO_2 film sensitivity towards CO and H_2 gases at different operating temperatures.

Fig. (8): TiO$_2$ film response time towards CO and H$_2$ gases at different operating Temperatures.

3.3.2. Hydrogen and oxygen
a) dynamic response

A representative curve for the sample response for Hydrogen at high and low operating temperatures (400 and 275°C) is shown in Fig.(7). The observed slight increase in film resistance at the onset of the curve tending to vanish at higher operating temperatures is mostly as observed in the case of CO gas sensing. This could be attributed to the slight decrease in the operating temperature, due to rushing of the test gas at the first moments of its entrance, allowing a corresponding slight increase in the film resistance. The (on-off) cycle of the gas is well defined which is not observed in the case of CO gas. The repeatable cycles support the sensing phenomena exerted by the film.

The dynamic response for oxygen gas is shown in Fig.(8). It is clear that the film resistance show sharp increase at the entrance (on) of the oxygen gas, which is not as the CO and H$_2$ gas, followed by a slow decrease in the film resistance in case of closing the gas (off). The increase in film resistance when exposed to oxygen gas and the decrease of it in case of CO and H$_2$ support the behaviour of TiO$_2$ as an n-type semiconductor.

b) Sensitivity and response time

The film sensitivity to sensing and response time for CO and H$_2$ with different operating temperatures is shown in Fig.(10). The higher sensitivity for H$_2$ is found to be at 330°C while for CO is at 310°C (Fig.10). The response time for CO and H$_2$ is random, but at lower operating temperature, the response time is shorter for CO (~ 3 sec.) than that for H$_2$ (~ 7 sec.).

c) Sensitivity mechanism

Since the film measurements are conducted in atmospheres almost without oxygen (Nitrogen ambient), the increase in film conductivity can not be due to hydrogen removing oxygen from the lattice [17,18,19] or the removal of chemisorbed oxygen [20,21,22]. It is likely that the hydrogen molecules get dissociated at the defects on the film surface. The molecules can diffuse into the lattice, and act as electron donors [23,24,25]. But this process would lead to very slow response and recovery time and complete recovery would be difficult.

Since, the investigated film almost regains its original resistance with hydrogen cycling; it appears that this is not the dominant mechanism behind hydrogen sensitivity. Hence, we suspect that the probable interaction between the film surface and hydrogen is the chemisorptions of the dissociated hydrogen on the film surface. During chemisorptions, hydrogen acts as a surface state and a partial charge transfer takes place from hydrogen to the conduction band of TiO$_2$ film. This creates an electron increase that enhances the film electrical conductance. On removing the hydrogen (off), electron transfer takes place back to hydrogen and it desorbs, thus, restoring the original resistance of the film.

On exposing the film to oxygen ambient (on), the lattice re-oxidizes takes electrons from the conduction band and, hence, the film conductivity decreases. On removing oxygen (off), the reduction of the lattice will not immediately occur. Therefore, the film requires several hours to restore its original conductivity.

4. Conclusion:

In the present work, it has been demonstrated a way to produce nano-sized TiO$_2$ films with only anatase phase through spray pyrolysis technique. This technique could be applied to extensive and low-cost production.

Film structure management (amorphous, crystalline and crystallite size) could be achieved by the control of the technique parameter (temperature and time). Qualitative agreement between structural features and electrical response

is inferred. The film resistance shows drastic and fast response to CO, H_2 and O_2. The film sensitivity and response time for each gas is calculated and traced as a function of operating temperature. Many mechanisms are discussed to explain the obtained results. The prepared TiO_2 films offer promising perspectives for gas sensing applications.

References

1. Hong-Ming Lin, Chia-His Keng and Chiun-Yen Tung., *Nanostrustured materials*, **9**, 747 (1997).
2. P. T. Moseley and B.C. Tofield, *"Solid State Gas Sensors"*, Adam Hilger imprint by IOP Publishing Ltd techno House, Redcliff Way Bristol BSI 6NX, England 242 Cherry Street, Philadelphia, PA 19106, USA, 56,126-127 (1987).
3. L.D. Birkefeld, A.M. Azad and S.A. Akbar, *J. Am. Ceram. Soc.,* **75**, 2961 (1992).
4. J. Hunsko, V. Lantto and H. Torvela, *Sens. Actuators B,* **16**, 245 (1993).
5. Fa-Min Liu and Tian-Min Wang, *Applied Surface Science,* **195**, 284 (2002).
6. K. Zakrzewska, A. Brudnik, M. Radecka and W. Posadowski, *Thin Solid Films,* **343/344**, 152 (1999).
7. D. Wicaksana, A. Kobayashi and A. Kinbara, *J. Vac. Sci. Technol.,* **A10**, 1479 (1992).
8. L. Castaňeda, J.C. Alonso, A. Ortiz, E. Andrade, J.M. Saniger and J.G. Baňuelos, *Materials Chemistry and Physics,* **77**, 938 (2002).
9. G. San Vicente, A. Morales and M.t. Gutierrez, *Thin Solid Films,* **391**, 133 (2001).
10. R. Roy and W.B. White, *J. Cryst. Growth,* **13/14**, 78 (1972).
11. B.D. Cullity, *"Elements of x-ray diffraction"*, Addison-Wesley Publishing Company Inc., London (1978).
12. R.K. Sharma, M.C. Bhatanger and G.L. Sharma, *Sensors and Actuators B,* **45**, 209 (1997).
13. H. Tang, K. Prasad, R. Sanjinès and F. Levy, *Sensors and Actuators B,* **71**, 26 (1995).
14. E. Comini, V. Guidi, C. Frigeri, I. Ricco and G. Sberveglieri, *Sensors and Actuators B,* **77**, 16 (2001).
15. P. T. Moseley, J.O.W. Norris and D. E. Williams, *"The techniques and Mechanical In Gas Sensing",* 194 (1991)
16. O.K. Varghese, D. Gong, M. Paulose, K.G. Ong and C.A. Grimes, *Sensors and Actuators B,* **93**, 338 (2003).
17. R.D. Shanonon, *J. Appl. Phys.,* **35**, 3414 (1964).
18. K.H. Kim, E.J. Ju and J.S. Choi, *J. Phys. Chem. Solid,* **45**, 1265 (1984).

19. G.C. Mather, F.M.B. Marques, J.R. Frade, *J. Eur. Ceram. Soc.,* **19**, 887 (1999).
20. R.M. Walton, D.J. Dwyer, J.W. Schwank, J.L. Gland, *Appl. Surf. Sci.,* **125**, 199 (1998).
21. M.J. Madou, S.R. Morrison, *"Chemical Sensing with Solid state Devices"*, Academic Press, New Yourk, (1989).
22. G.B. Raupp, J.A. Dumesic, *J. Phys. Chem.,* **89**, 5240 (1985).
23. L.D. Birkefeld, A.M. Azad, S.A. Akbar, *J. Am. Ceram. Soc.,* **75**, 2964 (1992).
24. J.B. Bates, J.C. Wang, R.A. Perkins, *Phys. Rev. B,* **19**, 4130 (1979).
25. G.J. Hill, *Br. J. Appl. Phys.,* **1**, 1151 (1968).